Substitution of the Conserved Arg-Tyr Dyad Selectively Disrupts the Hydrolysis Phase of the IMP Dehydrogenase Reaction†

Yollete V. Guillén Schlippe,‡ Thomas V. Riera,‡ Mohammad R. Seyedsayamdost,§ and Lizbeth Hedstrom*

Department of Biochemistry, Brandeis University, Waltham, Massachusetts 02454

Received October 8, 2003; Revised Manuscript Received February 17, 2004

ABSTRACT: Inosine 5′-monophosphate dehydrogenase (IMPDH) catalyzes the oxidation of IMP to XMP via the covalent E−XMP* intermediate (E−XMP*), with the concomitant reduction of NAD^+. Hydrolysis of E−XMP* is rate-limiting, and the catalytic base required for this step has not been identified. An X-ray crystal structure of *Tritrichomonas foetus* IMPDH with mizoribine monophosphate (MZP) reveals a novel closed conformation in which a mobile flap occupies the NAD^+/NADH site [Gan, L., Seyedsayamdost, M. R., Shuto, S., Matsuda, A., Petsko, G. A., and Hedstrom, L. (2003) *Biochemistry 42*, 857−863]. In this complex, a water molecule is coordinated between flap residues Arg418 and Tyr419 and MZP in a geometry that resembles the transition state for hydrolysis of E−XMP*, which suggests that the Arg418-Tyr419 dyad activates water. We constructed and characterized two point mutants, Arg418Ala and Tyr419Phe, to probe the role of the Arg418-Tyr419 dyad in the IMPDH reaction. Arg418Ala and Tyr419Phe decrease k_{cat} by factors of 500 and 10, respectively, but have no effect on hydride transfer or NADH release. In addition, the mutants display increased solvent isotope effects and increased levels of steady-state accumulation of E−XMP*. Inhibitor analysis indicates that the mutations destabilize the closed conformation, but this effect can account for a decrease in k_{cat} of no more than a factor of 2. These observations demonstrate that both the Arg418Ala and Tyr419Phe mutations selectively impair hydrolysis of E−XMP* by disrupting the chemical transformation. Moreover, since the effects of the Tyr419Phe mutation are comparatively small, these experiments suggest that Arg418 acts as the base to activate water.

Inosine 5′-monophosphate dehydrogenase (IMPDH)[1] catalyzes the oxidation of IMP to XMP with the concomitant reduction of NAD^+. This is the rate-limiting and first committed step in *de novo* guanine nucleotide biosynthesis. Inhibitors of IMPDH have antiproliferative activity and have been developed as immunosuppressive (*1*), anticancer (*2*), and antiviral agents (*3*−*6*). The conversion of IMP to XMP proceeds by two different reactions: oxidation and hydrolysis (*7*). In the oxidation reaction, the active site Cys319 (*Tritrichomonas foetus* IMPDH numbering) attacks the C-2 position of IMP and a hydride is transferred to NAD^+, forming NADH and the covalent E−XMP* intermediate (E−XMP*). In the hydrolysis reaction, E−XMP* is hydrolyzed after NADH release, producing XMP (Figure 1).

Enzymatic hydrolysis reactions generally require an enzymic base for activation of water. We have recently proposed that the conserved Arg418-Tyr419 dyad performs this role in the IMPDH reaction, based on our structure of the E·MZP complex, in which Cys319, MZP, and a water molecule are arranged in a tetrahedral geometry resembling the hydrolysis transition state (Figure 2) (*8*). The water molecule appears to be activated by hydrogen bonds to both Arg418 and Tyr419 (Figure 2). This observation is surprising because the solution pK_a's of both residues would seem to preclude this role (pK_a = 12.5 for Arg and 10.5 for Tyr). The Arg418-Tyr419 dyad is found on a mobile flap that is disordered in most IMPDH structures, including the E·IMP·β-Me-TAD complex (*9*), which suggests that the flap is disordered during the hydride transfer reaction. We propose that IMPDH undergoes a large conformational change in midcatalytic cycle: when NADH departs, the flap folds into the NADH site, positioning the Arg418-Tyr419 dyad for activation of water, thereby converting the enzyme from a dehydrogenase to a hydrolase.

Consistent with this model, the substitution of Arg418 with Ala decreases activity by a factor of 500 (*8*, *10*). We have previously shown that a burst of NADH production is observed in the reaction of Arg418Ala, which suggests that hydride transfer is not perturbed by this mutation (*8*). Here we report a detailed characterization of both the Arg418Ala and Tyr419Phe mutations. Both mutations selectively disrupt the hydrolysis reaction, and this decrease can be attributed

† Supported by NIH Grant GM54403 (L.H.) and NIH Training Grant GM08417 (Y.V.G.S. and T.V.R.).

* To whom correspondence should be addressed. Telephone: (781) 736-2333. Fax: (781) 736-2349. E-mail: hedstrom@brandeis.edu.

‡ These authors contributed equally to this work.

§ Present address: Department of Chemistry, Massachusetts Institute of Technology, Cambridge, MA 02139.

[1] Abbreviations: IMPDH, inosine 5′-monophosphate dehydrogenase; IMP, inosine 5′-monophosphate; NAD^+, nicotinamide adenine dinucleotide; NADH, reduced nicotinamide adenine dinucleotide; XMP, xanthosine 5′-monophosphate; LDH, lactic dehydrogenase; MZP, mizoribine monophosphate; ADP, adenosine 5′-diphosphate; tiazofurin, 2-β-D-ribofuranosylthiazole 4-carboxamide; β-Me-TAD, β-methylene thiazole-4-carboxamide adenine dinucleotide; MPA, mycophenolic acid; EICARMP, 5-ethynyl-1-β-D-ribofuranosylimidazole-4-carboxamide 5′-monophosphate; DTT, dithiothreitol.

10.1021/bi035823q CCC: $27.50
Published on Web 03/26/2004

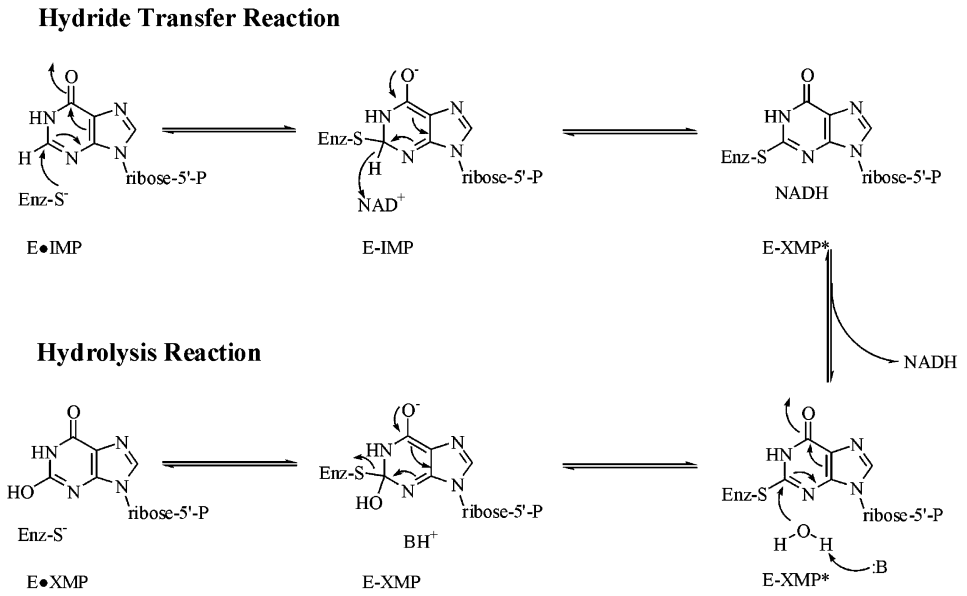

FIGURE 1: Chemical mechanism of IMPDH. In the hydride transfer reaction, the active site Cys attacks C-2 of IMP with expulsion of hydride to NAD^+ to form E−XMP* and NADH. NADH is released before the hydrolysis reaction takes place. The hydrolysis of E−XMP* requires a base to activate the catalytic water. The XMP tautomer shown bound to the enzyme is chosen arbitrarily.

to the rate of the chemical transformation rather than perturbation of the conformational change. Interestingly, the effects of the Arg418Ala mutation are much greater in magnitude than those of Tyr419Phe, and similar in magnitude to the effects of substitution of catalytic bases in other enzymes. Therefore, we propose that Arg418 is the catalytic base in the IMPDH reaction.

MATERIALS AND METHODS

Materials. IMP, ADP, NADH, MPA, and Tris were purchased from Sigma (St. Louis, MO). NAD^+ was purchased from Boehringer Mannheim. DTT was purchased from Research Organics, Inc. Glycerin, EDTA, trichloroacetic acid, and KCl were purchased from Fisher. [8-^{14}C]-IMP was obtained from Moravek Biochemicals, Inc. D_2O and DCl were purchased from Cambridge Isotope Laboratories, Inc. LDH (bovine heart) was purchased from ICN Biomedicals, Inc. Tiazofurin was obtained from the National Cancer Institute. EICARMP and MZP (*11*) were a gift from A. Matsuda (Hokkaido University, Hokkaido, Japan). Oligonucleotides were purchased from Operon.

Site-Directed Mutagenesis. The Arg418Ala and Tyr419Phe mutations were constructed in pTf1 which contains the *T. foetus* IMPDH gene in the pKK223-3 plasmid (*12*). Point mutations were created using the Quikchange kit (Stratagene, La Jolla, CA). The coding sequences were sequenced to ensure that there were no undesired mutations using a PRISM dye deoxy terminator cycle sequencing kit (Applied Biosystems, Inc.) and an Applied Biosystems 373A DNA sequencer at the Brandeis Sequencing Facility.

Expression and Purification. Plasmids containing the mutant IMPDH gene were transformed and expressed in *Escherichia coli* H712 cells, which lack their own IMPDH (*13*). Arg418Ala and Tyr419Phe were purified with a slight modification to the wild-type method (*12*). Both were initially purified using a Cibacron blue affinity resin. Arg418Ala was subsequently purified on a POROS HQ strong anion exchange column followed by a POROS HS strong cation exchange column. Tyr419Phe was further purified using a POROS HS strong cation exchange column followed by a POROS CM weak cation exchange column. The protein concentration was determined with the Bio-Rad assay with IgG as a standard dividing by a correction factor of 2.4 to account for the differences in chromophore generation between *T. foetus* IMPDH and IgG (unpublished results). In addition, the active sites of Tyr419Phe were titrated with EICARMP, which verified the protein concentration (*14*). The concentration of Arg418Ala was verified in the amplitudes of the pre-steady-state experiment, trapping E−XMP* and by titrating with MPA.

Enzyme Kinetics. Standard IMPDH assays contained 100 mM KCl, 3 mM EDTA, 1 mM DTT, and 50 mM Tris (pH 8.0) (assay buffer). NADH product inhibition was observed for Arg418Ala and overcome by adding saturating concentrations of LDH (20 μM). Tyr419Phe activity was determined by monitoring the absorbance of NADH at 340 nm (ϵ_{340} = 6.22 mM^{-1} cm^{-1}) on a Hitachi U-2000 UV−visible spectrophotometer at 25 °C. For the more inactive Arg418Ala, the fluorescence of NADH was monitored (λ_{ex} = 340 nm, λ_{em} = 460 nm) on a PerSeptive Biosystems Cytofluor II multiwell plate reader at 25 °C. Rates of NADH production were determined by calibration of the instrument with a standard curve of an NADH solution in assay buffer containing LDH. The presence of NAD^+ had no effect on the standard curve, confirming that NAD^+ does not compete with NADH for LDH at the concentrations used in the steady-state assays. Initial velocity data were fit by the Michaelis−Menten equation (eq 1) or an uncompetitive substrate inhibition equation (eq 2) using SigmaPlot (SPSS, Inc.):

$$v = V_m[\mathrm{IMP}]/(K_a + [\mathrm{IMP}]) \quad (1)$$

$$v = V_m/(1 + K_b/[\mathrm{NAD^+}] + [\mathrm{NAD^+}]/K_{ii}) \quad (2)$$

where v is the initial velocity, V_m is the maximal velocity,

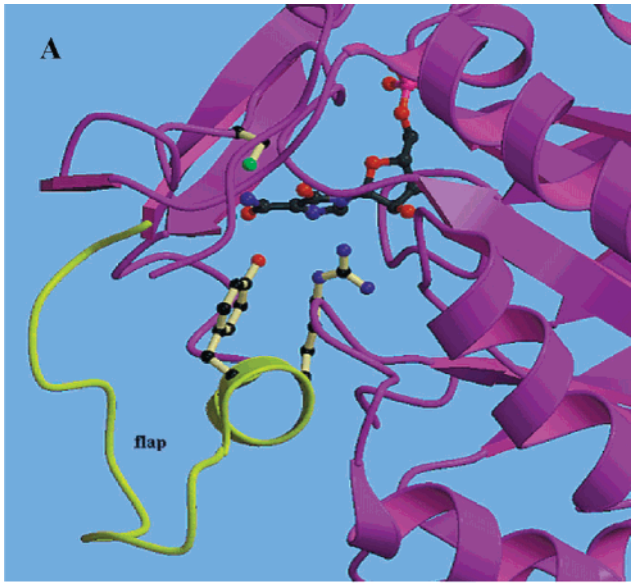

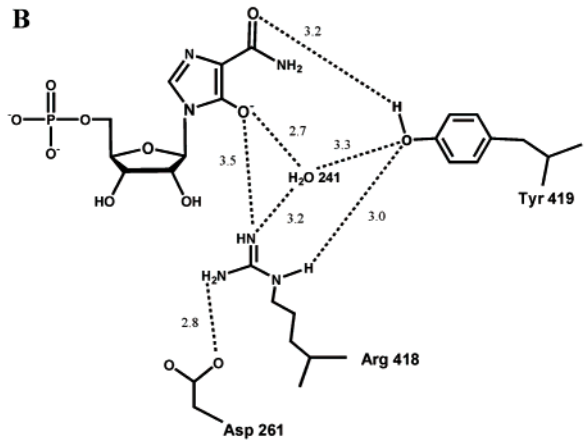

FIGURE 2: Interactions of the conserved Arg-Tyr dyad from the *T. foetus* IMPDH−MZP crystal structure (*8*). (A) The distal flap (yellow) adopts a closed conformation docking in the NAD^+ binding pocket. The side chains of Arg418, Tyr419, and Cys319 are shown as well as the inhibitor MZP. Atoms are colored as follows: black for C, blue for N, red for O, green for S, and magenta for P. This figure was generated by L. Gan with MolScript and rendered with Raster3D (*34*, *35*). (B) Schematic representation of the interactions between Arg418, Tyr419, water 241, MZP, and IMPDH. Distances between atoms are in angstroms.

K_a and K_b are the Michaelis constants for IMP and NAD^+, respectively, and K_{ii} is the substrate inhibition constant for NAD^+. Steady-state parameters with respect to NAD^+ were derived by first determining the apparent values of V_m for the initial velocity versus IMP plots (eq 1) and replotting these values against the NAD^+ concentration (eq 2). Similarly, the K_M value of IMP was derived by first determining the apparent values of V_m for the initial velocity versus NAD^+ concentration plots using eq 2 and replotting these values against the IMP concentration (eq 1).

Pre-steady-state experiments were performed using an Applied Photophysics SX.17MV stopped-flow spectrophotometer. NADH production was monitored by either absorbance (wavelength of 340 nm) or fluorescence (excitation wavelength of 340 nm, 420 nm cutoff emission filter) at 25 °C. Equal volumes of the enzyme and substrates were combined in assay buffer at time 0. For Arg418Ala, enzyme and saturating concentrations of IMP were preincubated, giving final concentrations of 100 μM IMP and 2.4 or 1 μM enzyme for absorbance and fluorescence experiments, respectively. The same starting complex for Tyr419Phe used final concentrations of 300 μM IMP and 1.6 or 0.4 μM enzyme for absorbance and fluorescence experiments, respectively.

Progress curves were fit with either a single-exponential (eq 3) or double-exponential (eq 4) equation with a steady-state term:

$$S_t = A_1[1 - \exp(-k_{obs1}t)] + vt + b \quad (3)$$

$$S_t = A_1[1 - \exp(-k_{obs1}t)] + A_2[1 - \exp(-k_{obs2}t)] + vt + b \quad (4)$$

where S_t is the signal at time t, A_1 and A_2 are the amplitudes of the first and second phases, respectively, k_{obs1} and k_{obs2} are the observed first-order rate constants for the first and second phases, respectively, v is the steady-state rate of the linear increase in absorbance or fluorescence, and b is the background signal at time 0. The hyperbolic dependence of k_{obs} on substrate concentration was fit by eq 5:

$$k_{obs} = k_{burst}S/(K_{app} + S) \quad (5)$$

where k_{burst} is the maximal value of k_{obs}, S is the concentration of the varied substrate, and K_{app} is the concentration of S at $^1/_2k_{burst}$. In addition, Dynafit (*15*) was used to globally fit the combined absorbance and fluorescence progress curves to the mechanism of Scheme 1 to derive values for the individual rate constants as described in the Supporting Information. XMP binding was assessed by following the intrinsic protein fluorescence as previously described (*12*).

Equilibrium Dissociation Constants (K_d). Dissociation constants for the interaction of ligands with enzyme were determined by following the quenching of the intrinsic protein fluorescence. The measurements were performed on a Hitachi F-2000 fluorescence spectrophotometer. Experiments were performed at 25 °C using excitation wavelengths of 295 nm when NAD^+ was titrated and 280 nm when IMP was titrated. Fluorescence values were corrected for inner filter effects by the formula

$$F_c = F_{obs}\,\text{antilog}[(A_{ex} + A_{em})/2] \quad (6)$$

where F_c is the corrected intensity, F_{obs} is the measured intensity, and A_{ex} and A_{em} are the absorbances at the excitation and emission wavelengths, respectively. Dynafit (*15*) was used to fit F_c and the ligand concentration to a simple one-step binding mechanism for Arg418Ala.

Inhibitor Kinetics. K_i determinations for mycophenolic acid (MPA), tiazofurin, and ADP for Tyr419Phe were performed with saturating IMP and varied NAD^+ and inhibitor concentrations. Because of the extremely low activity of Arg418Ala, substrate concentrations were held constant at 200 μM IMP and 20 μM NAD^+ and only the inhibitor concentration was varied. Multiple inhibitor experiments with tiazofurin and ADP were performed at constant IMP (as described above) and NAD^+ concentrations (20 and 200 μM for Arg418Ala and Tyr419Phe, respectively).

MZP inhibition was assessed in the presence of constant NAD^+ (50 and 250 μM for Arg418Ala and Tyr419Phe,

Scheme 1: Kinetic Scheme for *T. foetus* IMPDH (modified from that in ref *12*)

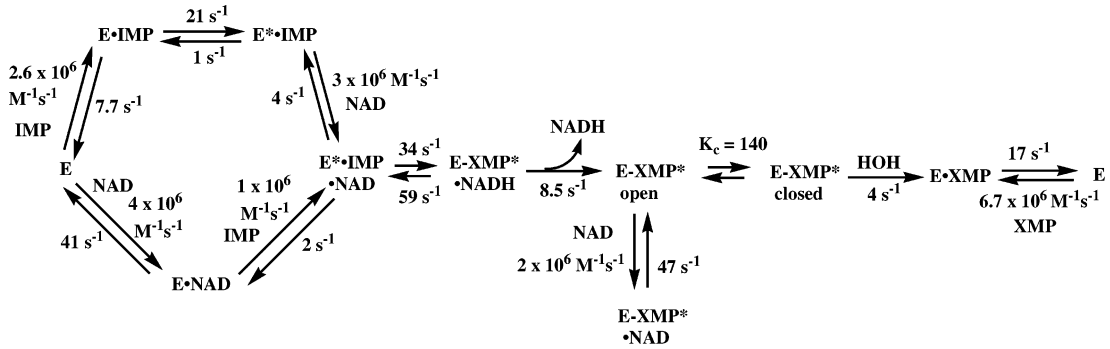

respectively) and varied IMP and inhibitor concentrations. MZP exhibited slow, tight binding to Tyr419Phe, so in this case, enzyme, IMP, and MZP were equilibrated by incubation for 20 min before the reaction with NAD^+ was initiated. All experiments were performed at 25 °C in assay buffer, and the initial velocities were fit by eq 9. LDH was present in Arg418Ala reaction mixtures to abate NADH product inhibition.

Data Analysis for Inhibitor Studies. The initial rate data were fit using SigmaPlot (SPSS, Inc.). Inhibition models were evaluated on the basis of the standard errors of the fitted parameters.

noncompetitive inhibition

$$v = V_m[NAD^+]/[K_{M(NAD)}(1 + I/K_{is}) + [NAD^+](1 + I/K_{ii})] \quad (7)$$

uncompetitive, tight-binding inhibition

$$v = (v_0/2E)\{E - I - K_{app} + [(E - I - K_{app})^2 + 4EK_{app}]^{0.5}\} \quad (8)$$

where $K_{app} = K_{ii}[K_{M(NAD)}/[NAD^+] + 1]$

competitive, tight-binding inhibition

$$v = (v_0/2E)\{E - I - K_{app} + [(E - I - K_{app})^2 + 4EK_{app}]^{0.5}\} \quad (9)$$

where $K_{app} = K_{is}[[IMP]/K_{M(IMP)} + 1]$

multiple inhibition

$$v = v_0/[1 + I/K_i + J/K_j + IJ/\alpha K_i K_j] \quad (10)$$

In eqs 7−10, v is the initial velocity, S is the concentration of substrate, I is the concentration of free inhibitor (which is equivalent to the total inhibitor concentration in eqs 7 and 10), V_m is the maximal velocity, K_{is} and K_{ii} are the slope and intercept inhibition constants, respectively, v_0 is the initial velocity in the absence of inhibitor, E is the enzyme concentration, K_i and K_j are the inhibition constants for inhibitors I and J, respectively, and α is the interaction constant for the interaction between inhibitors I and J.

Complete data sets varying both inhibitor and substrate concentrations were collected for Tyr419Phe and fit to each equation to determine the best inhibition model. However, the low activity of Arg418Ala permits variation of only the inhibitor concentration, so inhibition was analyzed using Dynafit (*15*) assuming the same mechanism of inhibition as observed in the wild type and Tyr419Phe.

Labeling IMPDH with [^{14}C]IMP. Reaction mixtures contained 4.5 or 2.5 μM enzyme, 60 or 50 μM [8-^{14}C]IMP, and 75 or 250 μM NAD^+ for Arg418Ala or Tyr419Phe, respectively, in assay buffer at 25 °C. Enzyme, [8-^{14}C]IMP, and NAD^+ were mixed, and reactions were quenched during the steady-state phase by precipitation with TCA to a final concentration of 10%. The enzyme samples were collected on 0.45 μm HA nitrocellulose filters (Millipore) and washed with 10% TCA. Radioactivity was measured using a scintillation counter. Control reactions in which NAD^+ or enzyme was omitted from the assay mixture were performed for each experiment.

Solvent Deuterium Isotope Effects. Assay buffer was prepared in D_2O or H_2O. The pH meter readings were corrected for the D_2O effect by adding 0.4 throughout. Activity was assayed by holding the IMP concentration at 100 μM and varying the NAD^+ concentration appropriately for determination of V_m. The reactions were initiated by the addition of enzyme, and the production of NADH was monitored by the absorbance (Tyr419Phe and wild type) or fluorescence (Arg418Ala).

RESULTS

Kinetic Mechanism of Wild-Type IMPDH. We previously derived a model for the kinetic mechanism of wild-type IMPDH (*12*). The key features of this mechanism are random addition of substrates and fast and reversible hydride transfer followed by slow NADH release which precedes the slow hydrolysis of the E−XMP* intermediate. In addition, NAD^+ inhibits the reaction by forming the dead-end E−XMP*•NAD^+ complex. We have further refined this model to include a rapid conformational change prior to hydrolysis of E−XMP* as indicated by our recent results (*8*). The determination of the equilibrium constant K_c for this conformational change is described below. In addition, we have globally fit reaction progress curves monitored using Dynafit as described in the Supporting Information. The values derived in the global fit are in good agreement with those reported previously (*12*). Scheme 1 summarizes our current model for the wild-type reaction.

Steady-State Characterization of Arg418Ala and Tyr419Phe. We constructed two point mutants, Arg418Ala and Tyr419Phe, in *T. foetus* IMPDH to probe the role of the Arg418-Tyr419 dyad in the IMPDH reaction. Several predictions can be made

Table 1: Steady-State Parameters of *T. foetus* IMPDH and Mutants

	K_M(IMP) (μM)	K_M(NAD$^+$) (μM)	K_{ii}(NAD$^+$) (mM)	k_{cat} (s^{-1})	$^{H_2O}k_{cat}/^{D_2O}k_{cat}$
wild type	1.7 ± 0.4[a]	150 ± 30[a]	6.8 ± 1.8[a]	1.9 ± 0.2[a]	1.6 ± 0.1
Arg418Ala	3 ± 3	1.6 ± 0.3	0.11 ± 0.01	0.004 ± 0.0004	5 ± 2
Tyr419Phe	0.7 ± 0.9	70 ± 10	1.1 ± 0.2	0.22 ± 0.01	2.4 ± 0.3

[a] From ref *12*.

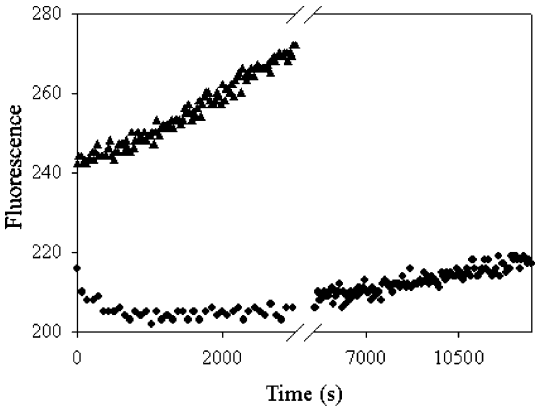

FIGURE 3: Effect of LDH on the Arg418Ala reaction. Arg418Ala exhibits severe NADH inhibition in the absence of LDH (●). When saturating concentrations of LDH are present [20 μM, K_d = 1.5 μM (*33*)] (▲), the fluorescence signal increases 3-fold and the initial rate doubles.

if hydrolysis is selectively perturbed by removal of the catalytic base. (1) Hydrolysis should be inhibited by a factor of at least 100 and will become solely rate-limiting, resulting in a significant drop in k_{cat}. (2) The fraction of enzyme that accumulates as E−XMP* should increase to ∼1. (3) More pronounced NAD$^+$ substrate inhibition will be observed due to the increase in the level of E−XMP* accumulation. (4) The solvent deuterium isotope effect should increase since hydrolysis will be completely rate-limiting. (5) Ideally, hydride transfer and NADH release will not be perturbed. Both mutations fulfill all of the predictions listed above, which indicates that the Arg418-Tyr419 dyad is selectively involved in the hydrolysis reaction.

The steady-state parameters for both mutants are listed in Table 1. Initial characterization revealed that Arg418Ala exhibits severe NADH product inhibition (Figure 3). This inhibition was relieved by trapping NADH with saturating concentrations of LDH (Figure 3). LDH also increases the fluorescence of NADH by ∼3-fold, resulting in a more sensitive assay (*16*). Note that the lag in Figure 3 is an artifact of the instrument; some time is required to produce detectable NADH levels. NADH product inhibition is not observed with Tyr419Phe under normal assay conditions, and LDH has no effect on the activity of this enzyme. In addition, LDH has no effect on the wild-type reaction (data not shown). Arg418Ala and Tyr419Phe decrease k_{cat} by factors of 500 and 10, respectively. Unfortunately, the values of K_m of IMP are too low to measure accurately. Both mutations decrease the value of K_{ii} for NAD$^+$ substrate inhibition (a factor of 65 for Arg418Ala and a factor of 7 for Tyr419Phe), as expected if hydrolysis becomes more rate-limiting, causing the E−XMP* intermediate to accumulate. However, the Arg418Ala mutation also decreases the value of K_M for NAD$^+$ by a factor of 93. Since K_M is a complex kinetic constant, this decrease could result from an increase in the affinity of the NAD$^+$ site or from other changes in the kinetic mechanism. Nevertheless, the steady-state kinetic properties of the two mutants are generally consistent with the proposal that the Arg418-Tyr419 dyad is selectively involved in the hydrolysis of E−XMP*. Interestingly, only the Arg418Ala mutation decreases k_{cat} by the magnitude expected for loss of the catalytic base.

Solvent Deuterium Isotope Effects. The experiments described above suggest that the mutations selectively decrease the rate of the hydrolysis reaction, which predicts that the solvent isotope effect on k_{cat} should increase. Table 1 shows that both mutations do indeed increase the solvent isotope effect, further suggesting that hydrolysis has become more rate-limiting.

Accumulation of E−XMP in Arg418Ala and Tyr419Phe.* If hydrolysis is rate-limiting as indicated above, then the mutant enzymes should accumulate in E−XMP* during the steady state. We measured the fraction of enzyme that is trapped as E−XMP* when the reaction was quenched with acid by monitoring the incorporation of radioactivity from [8-^{14}C]IMP into protein (see Materials and Methods). Under these conditions, the wild-type enzyme contains 0.5 equiv of E−XMP*, as expected given hydrolysis is only partially rate-limiting (*12*). For both mutants, all of the enzyme is trapped as E−XMP*: 1.0 ± 0.3 and 0.9 ± 0.2 equiv of E−XMP* contained in Arg418Ala and Tyr419Phe, respectively. This result is also consistent with rate-determining hydrolysis in the mutant enzymes.

Substrate and Product Binding with Arg418Ala. Because the value of K_M of NAD$^+$ decreased significantly in Arg418Ala, which could be associated with a perturbation of substrate binding, we determined the dissociation constants for both substrates. Both IMP and NAD$^+$ quench the intrinsic protein fluorescence of IMPDH, which provides a convenient assay for binding. The value of K_d for IMP did not change significantly for Arg418Ala ($K_d = 0.45 \pm 0.2$ μM vs K_d = 0.15 μM for the wild type), substantiating the conclusion that IMP binding is not perturbed by this mutation. However, unlike wild-type IMPDH which displays a sigmoidal binding curve for NAD$^+$ [K_1 = 340 μM and K_2 = 1600 μM with an overall K_d of 740 μM (*12*)], Arg418Ala displays a simple binding curve for NAD$^+$ with a K_d of 1900 ± 500 μM. This value is similar to the second dissociation constant of wild-type IMPDH, and also similar to the overall K_d. It is possible that the mutation changes the fluorescence properties so that we can no longer observe the first dissociation constant. In any case, we are unable to confirm that the Arg418Ala mutation increases the affinity of NAD$^+$, so the decrease in the K_M of NAD$^+$ may result from other changes in the kinetic mechanism.

To demonstrate that XMP release is faster than k_{cat}, we measured the kinetics of binding of XMP to Arg418Ala by monitoring changes in the intrinsic protein fluorescence as described previously for the wild type (*12*). XMP binds to

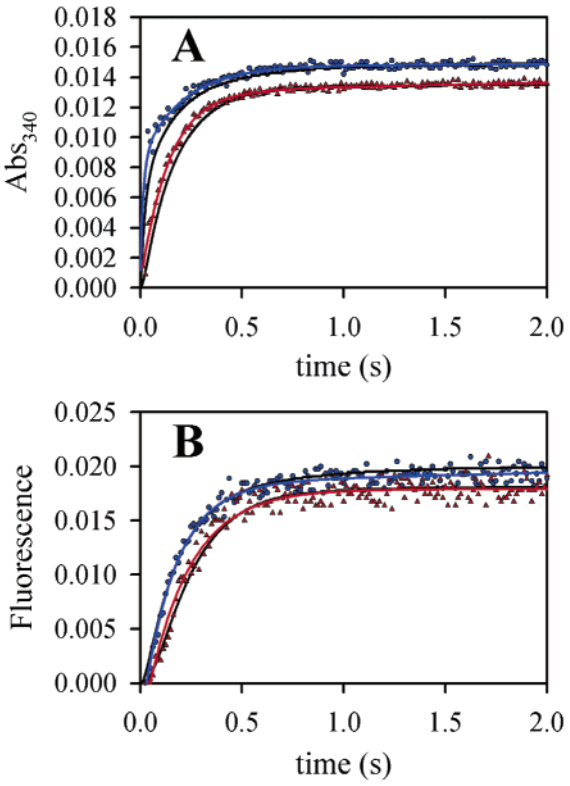

FIGURE 4: Progress curves for the Arg418Ala reaction as measured by stopped-flow absorbance and fluorescence spectroscopy. (A) Reaction of 2.4 μM enzyme preincubated with 100 μM IMP and mixed with 0.1 mM NAD^+ (triangles) or with 4 mM NAD^+ (circles) under standard assay conditions. The red and blue lines show the fit by a double exponential with a steady state (eq 4). The solid black lines represent the kinetic model and rate constants in Scheme 2 derived in global analysis using Dynafit. (B) Reaction of 1 μM enzyme preincubated with 97 μM IMP and mixed with 0.1 mM NAD^+ (triangles) or with 2 mM NAD^+ (circles) under standard assay conditions. Production of NADH was monitored by fluorescence and has been normalized with absorbance units. The blue and red lines show the fit by a single exponential with a steady state (eq 3). The solid black lines represent the kinetic model and rate constants in Scheme 2 derived in global analysis using Dynafit.

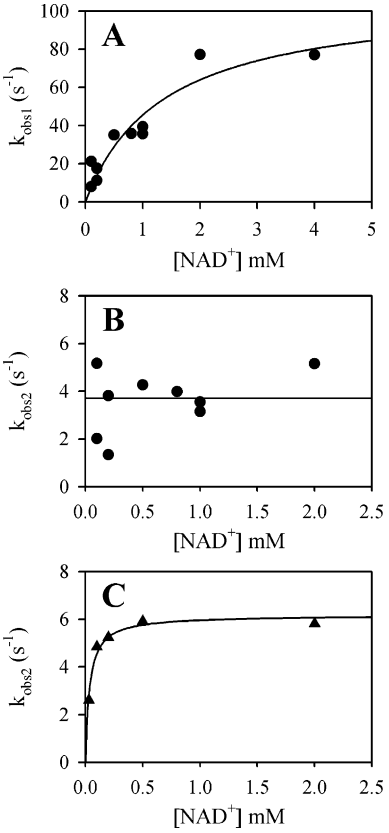

FIGURE 5: Pre-steady-state reaction of Arg418Ala. Progress curves for the reaction of E−IMP with varying concentrations of NAD^+ were collected as described in the legend of Figure 4 and Materials and Methods. The absorbance progress curves were fit by eq 4, which describes a double exponential and a steady state, while the fluorescence progress curves were fit by eq 3, which describes a single exponential with a steady state. Examples of reaction progress curves and fits can be found in Figure 4. (A) Dependence of k_{obs1} on NAD^+ concentration when absorbance is monitored. The line is the best fit of the data to eq 5. (B) Dependence of k_{obs2} on NAD^+ concentration when absorbance is monitored. The black line represents the average value of k_{obs2}. (C) Dependence of k_{obs} when fluorescence is monitored. The line is the best fit of the data to eq 5.

Arg418Ala in a single-exponential process. The values of k_{obs} are linearly dependent on XMP, and the values of k_{on} and k_{off} are similar to that of the wild type and much greater than k_{cat} [$k_{on} = (10 \pm 1) \times 10^6$ M^{-1} s^{-1} and $k_{off} = 10 \pm 5$ s^{-1} (data not shown) compared to $k_{on} = 6.7 \times 10^6$ M^{-1} s^{-1} and $k_{off} = 17$ s^{-1} for the wild type (*12*)]. This experiment demonstrates that XMP release is not rate-limiting in the Arg418Ala reaction.

Pre-Steady-State Reaction with Arg418Ala. We characterized the pre-steady-state IMPDH reaction to analyze the effects of Arg418Ala on hydride transfer and NADH release. Enzyme was preincubated with a saturating IMP concentration and mixed with varying concentrations of NAD^+. A pre-steady-state burst is observed when NADH production is monitored by absorbance. The progress curve has two exponential phases followed by a linear steady state (Figure 4A) and was fit by eq 4. The values of k_{obs1} display a hyperbolic dependence on NAD^+ concentration and were fit by eq 5 to give the maximal k_{burst1} value of 110 s^{-1} (Figure 5A). The value of k_{burst1} is similar to the maximal value of k_{burst1} in the wild-type reaction (62 s^{-1}) (*12*), which indicates that the rate of hydride transfer is similar to that of the wild type (only a single-exponential phase is observed in our previous experiments with the wild-type enzyme because NADH release is rate-limiting). In addition, the value of K_{app1} is similar to that of the wild type, which further suggests that the mutation has not perturbed NAD^+ binding (Table 2). The value of k_{obs2} did not vary with NAD^+ concentration, so the average value of 3.7 ± 0.4 s^{-1} was assigned to k_{burst2} (Figure 5B). The value of k_{burst2} is comparable to the wild-type rate constant for the release of NADH (8 s^{-1}) (Scheme 1).

We also monitored the reaction progress curve using fluorescence to assess the production of NADH (*12*). The fluorescence of NADH is quenched in the E−XMP*•NADH complex so that only free NADH is observed. The fluorescence progress curves were adequately fit with a single-exponential phase followed by a linear steady state as described by eq 3 (note that although a double exponential is expected, the quality of the data at early time points does not justify a higher parameter fit) (Figure 4B). The value of k_{obs} displays a hyperbolic dependence on NAD^+ concentration, as shown in Figure 5C, with a maximal k_{fluor2} of 6.2 s^{-1}. This value is similar to k_{burst2} from the absorbance

Table 2: Pre-Steady-State Reaction of Wild-Type and Mutant IMPDHs Monitored by Absorbance[a]

parameter	wild type[b]	Arg418Ala	Tyr419Phe
k_{burst1} (s^{-1})	62 ± 6	110 ± 20	>48[c]
K_{app1} (mM)	2.1 ± 0.5	1.4 ± 0.5	>20
k_{burst1}/K_{app1} (M^{-1} s^{-1})	3.0×10^4	7.9×10^4	$(2.3 \pm 0.1) \times 10^3$ [c]
Amp_1 ($[NADH]_1/[E]_{tot}$)[d]	0.45 ± 0.01	0.68 ± 0.07	≥0.5[e]
k_{burst2} (s^{-1})	na	3.7 ± 0.4[f]	5.3 ± 0.5
K_{app2} (mM)	na	<0.25	1.2 ± 0.4
k_{burst2}/K_{app2} (M^{-1} s^{-1})	na	$>2 \times 10^4$	4.4×10^3
Amp_2 ($[NADH]_2/[E]_{tot}$)[d]	na	0.35 ± 0.09	0.5[e]

[a] The absorbance time course displays two exponential phases followed by a linear steady state. These data were fit to eq 4. The rate constants for the exponential phases displayed a hyperbolic dependence on the NAD^+ concentration. k_{burst}, the maximum value of k_{obs}, was calculated from eq 5. na means not applicable. [b] From ref *12*. [c] The observed rate for the first exponential phase is linearly dependent on NAD^+ concentration up to 20 mM ($k_{obs1} = 48$ s^{-1}). The slope of this line is k_{burst1}/K_{app1}. [d] The concentration of NADH is calculated by $\Delta A_{340}/\epsilon l$, where ΔA_{340} is the absorbance amplitude of the burst phase, $\epsilon = 6.22$ mM^{-1} cm^{-1} for NADH, and l is the path length (1 cm). $[E]_{tot}$ is the total enzyme concentration. [e] The amplitude at the highest concentration (20 mM) of NAD^+ that was tested as explained in the text. [f] Average of k_{obs2}, as no NAD^+ dependence was observed as explained in the text.

Table 3: Kinetic Parameters for the Pre-Steady-State Reaction of Wild-Type and Mutant IMPDHs Monitored by Fluorescence

parameter	wild type[a]	Arg418Ala[b]	Tyr419Phe[c]
k_{fluor1} (s^{-1})	na[d]	na[d]	>48
k_{fluor2} (s^{-1})	6.5 ± 0.3	6.2 ± 0.2	5.7 ± 0.2
K_{app2} (mM)	2.4 ± 0.4	0.035 ± 0.006	0.7 ± 0.1
k_{fluor2}/K_{app2} (M^{-1} s^{-1})	2.7×10^3	1.8×10^5	8.1×10^3

[a] From ref *12*. [b] The fluorescence time course displayed a single-exponential phase followed by a linear steady state. The data were fit by eq 3. The rate constant for the exponential phase (k_{obs}) displayed a hyperbolic dependence on NAD^+ concentration. k_{fluor}, the maximum value of k_{obs}, was calculated from eq 5. [c] The fluorescence time course displays two exponential phases followed by a linear steady state. These data were fit by eq 4. The observed rate for the first exponential phase is linearly dependent on NAD^+ concentration up to 16 mM ($k_{obs1} = 48$ s^{-1}). The rate constant for the second phase displayed a hyperbolic dependence on the varied substrate, and k_{fluor} was calculated from eq 5. [d] Not applicable.

experiment and comparable to the value of k_{fluor} determined for the wild-type reaction (Table 3). This observation suggests that the rate of NADH release is also comparable to that of the wild type. We have confirmed these conclusions by deriving values for individual rate constants by globally fitting the absorbance and fluorescence progress curves using Dynafit as described in the Supporting Information. These experiments indicate that both hydride transfer and NADH release have not been affected by the Arg418Ala mutation and are much faster than k_{cat}, and confirm that hydrolysis is rate-limiting.

Pre-Steady-State Reaction with Tyr419Phe. The pre-steady-state reaction of Tyr419Phe was also examined to determine if the mutation affects either hydride transfer or NADH release. When the starting complex is E·IMP and the reaction is monitored by absorbance, a pre-steady-state burst exhibiting two exponential phases is observed followed by a steady state which is described by eq 4. The value of k_{obs1} is linearly dependent on NAD^+ concentration up to 20 mM, where $k_{obs1} = 48$ s^{-1} (Figure 6A). The slope of this line (k_{burst1}/K_{app1}) equals 2300 M^{-1} s^{-1} (Table 2) which is

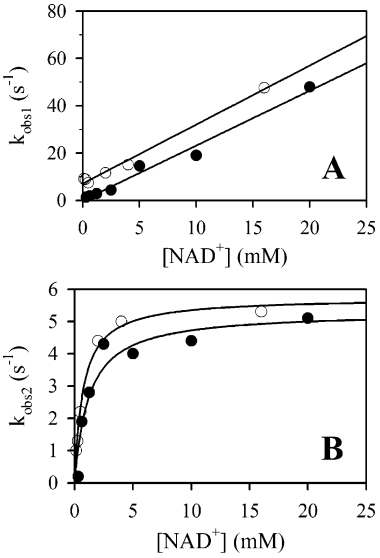

FIGURE 6: Pre-steady-state reaction of Tyr419Phe. Progress curves for the reaction of E−IMP with varying concentrations of NAD were collected as described in Materials and Methods. The values of k_{obs} were calculated from eq 4 for the absorbance (●) and fluorescence (○) experiments. (A) Linear dependence of k_{obs1} on NAD^+ concentration. (B) Hyperbolic dependence of k_{obs2} on NAD^+ concentration.

lower than the wild-type and Arg418Ala values by factors of 13 and 34, respectively. For the second phase, k_{obs2} exhibits a hyperbolic dependence on NAD^+ concentration, where $k_{burst2} = 5.3$ s^{-1} and $K_{app2} = 1.2$ mM (Figure 6B and Table 2).

At low concentrations of NAD^+, the rate constants for each phase are similar, making the amplitude for each phase difficult to distinguish. Consequently, trends in the individual amplitudes are obscured. However, the total amplitude for each NAD^+ concentration is ∼1 equiv. At the highest concentration of NAD^+ that was tested, where k_{obs1} is 10-fold greater than k_{obs2}, the individual amplitudes are easily distinguished and are 0.5 equiv for each phase (Table 2).

Two exponential phases are also observed when the production of NADH is monitored by fluorescence: the time course displays a lag followed by a burst and a linear steady-state phase (Table 3). The lag phase is linearly dependent on NAD^+ concentration up to 16 mM, where $k_{obs1} = 48$ s^{-1}, with a slope of 2600 M^{-1} s^{-1} (Figure 6A). This is identical to the k_{burst1}/K_{app1} value measured by absorbance. The burst phase shows a hyperbolic dependence on NAD^+ concentration with a k_{fluor2} of 5.7 s^{-1} and a K_{app2} of 0.7 mM (Table 3 and Figure 6B). These values are identical to k_{burst2} and K_{app2} from the absorbance experiment. Since the maximal values of both phases (≫48 and ∼5 s^{-1}) are similar to those of the wild type and much greater than k_{cat}, these experiments indicate that both hydride transfer and NADH release have not been affected by the Tyr419Phe mutation and indicate that hydrolysis is rate-limiting. We have confirmed these conclusions by deriving values for individual rate constants in global fits of the absorbance and fluorescence progress curves using Dynafit as described in the Supporting Information.

MPA Inhibition. In our model, the active site flap must fold into the NAD^+ site for hydrolysis of E−XMP* to occur (Scheme 2). Therefore, Arg418Ala and Tyr419Phe could

Scheme 2: Mechanistic Rate Constants

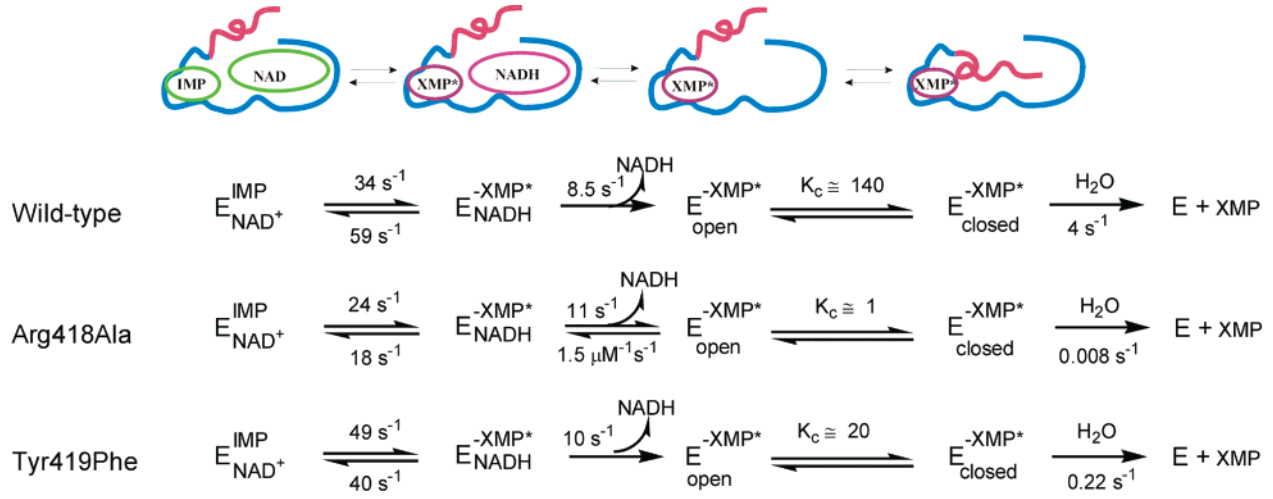

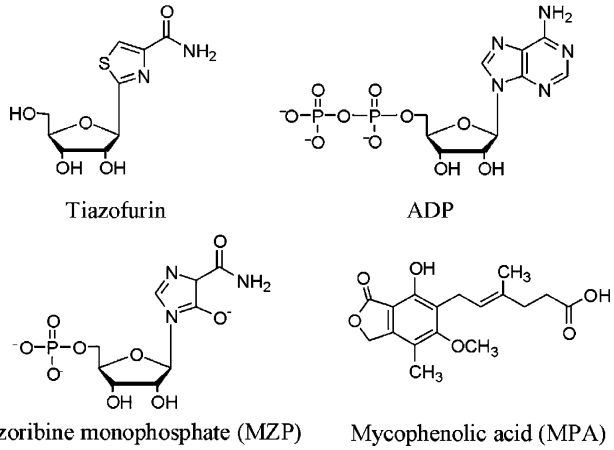

FIGURE 7: Structures of IMPDH inhibitors.

perturb the equilibrium between open and closed conformations as well as the actual hydrolysis reaction. This conformational effect can be assessed by monitoring MPA inhibition (see Figure 7 for inhibitor structures). MPA traps E−XMP* by binding in the nicotinamide end of the NAD^+ site (*17*−*20*). Thus, MPA competes with the flap for the NAD^+ site so that a shift toward the open conformation will increase the potency of MPA (*8*). Neither Arg418 nor Tyr419 contacts MPA; indeed, each is disordered in the MPA complex (*21*, *22*). Therefore, changes in the K_i of MPA will reflect changes in the equilibrium between the open and closed forms. Arg418Ala and Tyr419Phe increase the affinity of MPA by 29- and 18-fold, respectively (Table 4). This increase in potency must result from a change in the conformational equilibrium that favors the open state.

Tiazofurin and ADP Inhibition. Tiazofurin and ADP are weak inhibitors of the wild-type IMPDH that bind in the nicotinamide and adenosine subsites of the dinucleotide site, respectively (Table 4) (*19*, *23*). Both the Arg418Ala and Tyr419Phe mutations increase the potency of tiazofurin and ADP (Tables 4 and 5). Like MPA, neither tiazofurin nor ADP contacts the Arg418-Tyr419 dyad. Therefore, this increase in potency must also be attributed to an increase in the level of the open conformation.

The equilibrium between the open and closed conformations can also be assessed in a multiple-inhibitor experiment. In *T. foetus* IMPDH, tiazofurin and ADP are strongly synergistic with an interaction constant α of 0.007 (see eq 10) (*23*). A model for the interaction between tiazofurin and ADP is shown in Figure 8. *T. foetus* IMPDH favors the closed conformation; the first inhibitor pulls the equilibrium to the open conformation, thus enhancing the binding of the second inhibitor. The Arg418Ala and Tyr419Phe mutations increase the values of α by 60- and 6-fold, respectively, which further confirms that the equilibrium between the open and closed conformations is perturbed (Table 5).

MZP Inhibition. MZP induces the closed conformation and can be considered a transition-state analogue of the hydrolysis reaction (*8*, *24*). The Arg418Ala and Tyr419Phe mutations decrease the affinity of MZP by factors of ∼200 and 9, respectively (Table 4). However, because the Arg418-Tyr419 dyad contacts MZP, these decreases cannot be attributed simply to changes in the equilibrium between the open and closed conformations. The magnitude of the changes in MZP affinity is similar to the magnitude of the changes in the value of k_{cat}, as would be expected for a transition-state analogue.

DISCUSSION

The structure of E·MZP suggested that water is activated by a conserved Arg418-Tyr419 dyad located on a mobile flap (*8*). However, both of these residues have a high solution pK_a that would seem to preclude this role (pK_a = 12.5 for Arg and 10.5 for Tyr). The experiments reported here demonstrate that mutations of this dyad selectively disrupt the hydrolysis step. In Arg418Ala, the value of k_{cat} is decreased by a factor of 500, but the rates of hydride transfer and NADH release are comparable to that of the wild type. Similarly, in Tyr419Phe, the value of k_{cat} decreases by a factor of 10, but again hydride transfer and NADH release are comparable to those of the wild type. Increases in solvent isotope effects and the steady-state accumulation of E−XMP* further demonstrate that hydrolysis is rate-limiting in these mutants.

These observations are consistent with the proposal that the Arg418-Tyr419 dyad activates water. However, the hydrolysis reaction also requires a large conformational change (Scheme 2). The flap is open while the E·IMP·NAD^+ complex reacts to form the E−XMP*·NADH complex.

Table 4: Inhibition of Wild-Type and Mutant IMPDHs[a]

		wild type	Arg418Ala			Tyr419Phe		
inhibitor	constant	observed	observed	rel[b]	predicted[c]	observed	rel[b]	predicted[c]
MPA (μM)	K_{ii}	9[d] (UC)	0.31 ± 0.02[e] (TB)	29	0.1	0.51 ± 0.09 (UC, TB)	18	2
ADP (mM)	K_{is}	31[f] (C)	nd	na	0.4	4 ± 5 (NC)	8	5
	K_{ii}	na	nd	na	na	3 ± 1 (NC)	10	na
tiazofurin (mM)	K_{is}	50[f] (NC)	nd	na	0.7	14 ± 15 (NC)	4	8
	K_{ii}	69[f] (NC)	nd	na	1	11 ± 3 (NC)	6	12
NAD^+ (mM)	K_{ii}	6.8[g] (UC)	0.11 ± 0.01 (UC)	62	0.1	1.1 ± 0.2 (UC)	6	1.1
NADH (μM)	K_{ii}	240[f,k] (NC)	6.2 ± 0.2[h] (UC)	39	3	nd	na	40
MZP (nM)	K_{is}[i]	0.15[j] (C, S, TB)	28 ± 6 (C, TB)	na	na	1.3 ± 0.5 (C, S, TB)	na	na

[a] Experimental conditions: 50 mM Tris (pH 8.0), 100 mM KCl, 3 mM EDTA, and 1 mM DTT at 25 °C. The NAD^+ concentration was varied, while 200 and 100 μM IMP were used for Arg418Ala and Tyr419Phe, respectively. Inhibition constants and mechanism are with respect to NAD^+: C, competitive; UC, uncompetitive; NC, noncompetitive; TB, tight-binding; S, slow. na means not applicable and nd no data. [b] Calculated from K_{wt}/K_{mutant} in the same rows, except for ADP, for which K_{wt} is always K_{is} and for Arg418Ala tiazofurin where K_{iiwt} is divided by K_i from Table 5. [c] Predicted inhibition constant from $(\alpha_{wt}/\alpha_{mutant})K_{iwt}$. [d] From ref *32*. [e] Concentration of inhibitor which gives 50% inhibition (IC_{50}) from experiments in which only the inhibitor concentration was varied as explained in the text. [f] From ref *19*. [g] From ref *12*. [h] Calculated from k_7/K_i as described in the Supporting Information. [i] The IMP concentration was varied, and 50 and 250 μM NAD^+ were used for Arg418Ala and Tyr419Phe, respectively. Inhibition constant and mechanism with respect to IMP. [j] From ref *8*. [k] Measured at 37 °C.

Table 5: Multiple-Inhibition Experiments with Wild-Type and Mutant IMPDHs[a]

		wild type	Arg418Ala		Tyr419Phe	
inhibitor	constant	observed	observed	rel[b]	observed	rel[b]
ADP and tiazofurin	α	0.007[c]	0.5 ± 0.3	70	0.04 ± 0.02	6
ADP (mM)	K_i	nd	1.7 ± 0.5	20	4 ± 1	8
tiazofurin (mM)	K_j	nd	2.4 ± 0.5	30	11 ± 3	6

[a] Experimental conditions: 50 mM Tris (pH 8.0), 100 mM KCl, 3 mM EDTA, and 1 mM DTT at 25 °C. The substrate concentration was fixed at 200 and 100 μM IMP and 20 and 250 μM NAD^+ for Arg418Ala and Tyr419Phe, respectively. Inhibition constants were calculated from eq 10. [b] Calculated from $\alpha_{mutant}/\alpha_{wt}$ or K_{wt}/K_{mutant} using K_{is} for ADP and K_{ii} for tiazofurin from Table 4. [c] From ref *23*.

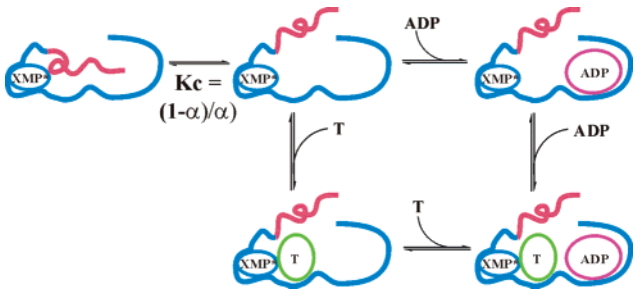

FIGURE 8: Model for the synergistic interaction of tiazofurin and ADP. The first inhibitor bound shifts the equilibrium to the open conformation. In this model, α represents the fraction of E−XMP* in the open conformation.

When NADH departs, the flap folds into the active site where the Arg418-Tyr419 dyad is positioned next to E−XMP*. It is possible that the Arg418-Tyr419 dyad induces the conformational change while some other residue activates water. Therefore, the effects on the conformational change must be uncoupled from the effects on the chemical transformation.

Inhibitors can be used to gauge the conformational effects. Inhibitors that bind in the dinucleotide site compete with the flap (e.g., MPA, NADH, NAD^+, tiazofurin, and ADP), and the potency of these inhibitors will increase if a mutation destabilizes the closed conformation. Neither Arg418 nor Tyr419 appears to contact MPA, NAD^+, or TAD, since the flap is disordered in these complexes (*9*, *20*−*22*). Therefore, changes in the affinity of MPA, NADH, NAD^+, tiazofurin, and ADP in response to mutations of Arg418 and Tyr419 must be attributed to changes in the conformational equilibrium. The potency of these inhibitors increases 20−60-fold in Arg418Ala (Table 4), which indicates this mutation destabilizes the closed conformation. This effect is much smaller than the effect on k_{cat} of a factor of 500. Therefore, the Arg418Ala mutation primarily impairs the chemical transformation. In contrast, the potency of MPA, NAD^+, tiazofurin, and ADP increases by a factor of 4−20 in Tyr419Phe, which is similar to the decrease by a factor of 10 in k_{cat}. With this reasoning, Tyr419 functions mainly in stabilizing the closed conformation. However, this analysis is incomplete because it only measures increases in the level of the open conformation, rather than changes in the conformational equilibrium, and thus overestimates the effects on k_{cat}. Therefore, while it is clear that the primary role of Arg418 is activation of water, the relative contributions of Tyr419 to water activation and the conformational change cannot be assessed by this method.

With three reasonable assumptions, the conformational equilibrium can be determined with the multiple-inhibitor experiment. (1) The conformational change is fast; this assumption is validated by the observation of solvent isotope effects on k_{cat} which indicates that the hydrolysis reaction is rate-limiting for wild-type and both mutant enzymes. (2) The conformational equilibrium is similar for all enzyme forms, e.g., E·IMP, E−XMP*, etc.; the similarity in the changes of potency for the various inhibitors (see above) validates this assumption. (3) Tiazofurin and ADP are intrinsically independent; i.e., for an enzyme entirely in the open conformation, $\alpha = 1$. Tiazofurin and ADP are independent inhibitors of human IMPDH type 2 which is believed to favor the open conformation (*8*, *23*), which validates this last assumption. With these assumptions, α becomes the fraction of enzyme in the open conformation, $1 - \alpha$ is the fraction in the closed conformation (Figure 8), and the equilibrium constants for the conformational change (K_{closed}) are 140, 1, and 20 for the wild type, Arg418Ala, and Tyr419Phe, respectively. The effects of the mutations on inhibitor potency can be calculated from these values of k_{closed} and are in good agreement with experimental observation (Table 4), which further validates this model. More importantly, if the mutations only impaired formation of the closed con-

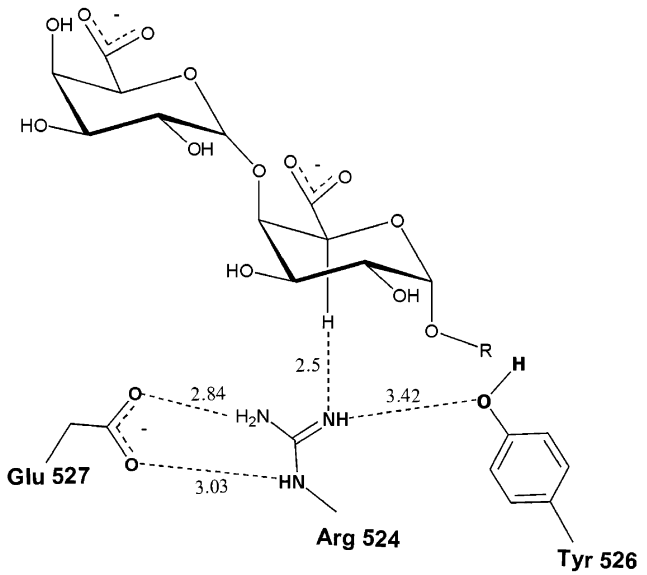

FIGURE 9: Active site of polygalacturonic acid lyase (PGAL). The complex with the substrate trigalacturonic acid (*30*) reveals a catalytic triad of Arg524, Tyr526, and Glu527 similar to that of IMPDH in complex with MZP (Figure 2). Distances between atoms are in angstroms.

formation, then modest decreases in k_{cat} would be observed (k_{cat} = 1.6 and 2.3 s^{-1} for Arg418Ala and Tyr419Phe, respectively, vs 2.4 s^{-1} for the wild type; see the Supporting Information for details). Therefore, the decreases by factors of 500 and 10 in k_{cat} in Arg418Ala and Tyr419Phe, respectively, cannot be attributed to an inability to form the closed conformation and instead must be assigned to disruption of the chemical transformation.

We have derived rate constants for the individual steps of the wild-type and mutant IMPDH reactions by globally fitting the pre-steady-state experiments as described in the Supporting Information. Scheme 2 shows the results of this analysis. Both mutations have negligible effects on the hydride transfer and NADH release steps and large effects on the conformational change and hydrolysis of E−XMP*. Both Arg418 and Tyr419 are in position to activate water directly (Figure 2). We believe that Tyr419 is not the catalytic base because the Tyr419Phe mutation only decreases the hydrolysis step by a factor of 20 (Scheme 2). Instead, Tyr419 may activate Arg418. Tyr419 also appears to be positioned to stabilize the oxyanion of the E−XMP intermediate (Figure 1). However, this hydrogen bond has poor geometry, so we believe the oxyanion is probably stabilized by the backbone NH group of Glu408 and Gly409. In contrast, Arg418Ala decreases the hydrolysis step by a factor of 10^3 (Scheme 2); similar decreases are observed when catalytic bases are removed in other hydrolases (*25*). Therefore, we believe that Arg418 is the catalytic base in the IMPDH reaction.

The proposition that Arg acts as a catalytic base is provocative because of its high pK_a in solution. While we have been unable to identify another enzyme that uses Arg to activate water, several appear to use Arg to abstract protons in elimination reactions: fumarate reductase (*26*, *27*), L-aspartate oxidase (*28*), tyrosine phenol-lyase (*29*), and polysaccharide lyase (*30*, *31*). Interestingly, polygalacturonic acid lyase (PGAL), a polysaccharide lyase, contains a catalytic triad of Arg524, Tyr526, and Glu527 with a geometry similar to that of Arg418, Tyr419, and Asp261 of IMPDH (compare Figures 2 and 9) (*30*), and mutations of Arg524 and Tyr526 in PGAL have effects on k_{cat} similar to those of the Arg418-Tyr419 mutations in IMPDH reported here (*30*). Perhaps these two different enzymes share a common mechanism for activation of the catalytic Arg.

ACKNOWLEDGMENT

We thank Satoshi Shuto for providing MZP and Akira Matsudafor providing EICARMP. We also acknowledge Lu Gan for generating Figure 2A as well as assistance with other figures and Becky Meyers of the Brandeis Core Facility for DNA sequencing.

SUPPORTING INFORMATION AVAILABLE

Pre-steady-state progress curve simulations, global fits, and discussion of the relationship between k_{cat} and α. This material is available free of charge via the Internet at http://pubs.acs.org.

REFERENCES

1. Allison, A. C., and Eugui, E. M. (1993) Immunosuppressive and other effects of mycophenolic acid and an ester prodrug, mycophenolate mofetil, *Immunol. Rev. 136*, 5−28.
2. Weber, G. (1983) Enzymes of purine metabolism in cancer, *Clin. Biochem. 16*, 57−63.
3. Robins, R. K., Revankar, G. R., McKernan, P. A., Murray, B. K., Kirsi, J. J., and North, J. A. (1985) The importance of IMP dehydrogenase inhibition in the broad spectrum antiviral activity of ribavirin and selenazofurin, *Adv. Enzyme Regul. 24*, 29−43.
4. Streeter, D. G., Witkowski, J. T., Khare, G. P., Sidwell, R. W., Bauer, R. J., Robins, R. K., and Simon, L. N. (1973) Mechanism of action of 1-β-D-ribofuranosyl-1,2,4-triazole-3-carboxamide (Virazole), a new broad-spectrum antiviral agent, *Proc. Natl. Acad. Sci. U.S.A. 70*, 1174−1178.
5. Jackson, R. C., Weber, G., and Morris, H. P. (1975) IMP dehydrogenase, an enzyme linked with proliferation and malignancy, *Nature 256*, 331−333.
6. Franchetti, P., and Grifantini, M. (1999) Nucleoside and non-nucleoside IMP dehydrogenase inhibitors as antitumor and antiviral agents, *Curr. Med. Chem. 6*, 599−614.
7. Hedstrom, L. (1999) IMP dehydrogenase: mechanism of action and inhibition, *Curr. Med. Chem. 6*, 545−560.
8. Gan, L., Seyedsayamdost, M. R., Shuto, S., Matsuda, A., Petsko, G. A., and Hedstrom, L. (2003) The immunosuppressive agent mizoribine monophosphate forms a transition state analogue complex with inosine monophosphate dehydrogenase, *Biochemistry 42*, 857−863.
9. Gan, L., Petsko, G. A., and Hedstrom, L. (2002) Crystal structure of a ternary complex of *Tritrichomonas foetus* inosine 5′-monophosphate dehydrogenase: NAD^+ orients the active site loop for catalysis, *Biochemistry 41*, 13309−13317.
10. Zhang, R., Evans, G., Rotella, F. J., Westbrook, E. M., Beno, D., Huberman, E., Joachimiak, A., and Collart, F. R. (1999) Characteristics and crystal structure of bacterial inosine-5′-monophosphate dehydrogenase, *Biochemistry 38*, 4691−4700.
11. Shuto, S., Haramuishi, K., Fukuoka, M., and Matsuda, A. (2000) Synthesis of sugar-modified analogs of bredinin (mizoribine), a clinically useful immunosuppressant, by a novel photochemical imidazole ring-cleavage reaction as the key step, *J. Chem. Soc., Perkin Trans. 1 21*, 3603−3609.
12. Digits, J. A., and Hedstrom, L. (1999) Kinetic mechanism of *Tritrichomonas foetus* inosine 5′-monophosphate dehydrogenase, *Biochemistry 38*, 2295−2306.
13. Nijkamp, H. J., and De Haan, P. G. (1967) Genetic and biochemical studies of the guanosine 5′-monophosphate pathway in *Escherichia coli*, *Biochim. Biophys. Acta 145*, 31−40.
14. Wang, W., Papov, V. V., Minakawa, N., Matsuda, A., Biemann, K., and Hedstrom, L. (1996) Inactivation of inosine 5′-monophosphate dehydrogenase by the antiviral agent 5-ethynyl-1-β-D-ribofuranosylimidazole-4-carboxamide 5′-monophosphate, *Biochemistry 35*, 95−101.

15. Kuzmic, P. (1996) Program DYNAFIT for the analysis of enzyme kinetic data: application to HIV proteinase, *Anal. Biochem. 237*, 260−273.
16. Whitaker, J. R., Yates, D. W., Bennett, N. G., Holbrook, J. J., and Gutfreund, H. (1974) The identification of intermediates in the reaction of pig heart lactate dehydrogenase with its substrates, *Biochem. J. 139*, 677−697.
17. Link, J. O., and Straub, K. (1996) Trapping of an IMP dehydrogenase-substrate covalent intermediate by mycophenolic acid, *J. Am. Chem. Soc. 118*, 2091−2092.
18. Verham, R., Meek, T. D., Hedstrom, L., and Wang, C. C. (1987) Purification, characterization, and kinetic analysis of inosine 5′-monophosphate dehydrogenase of *Tritrichomonas foetus*, *Mol. Biochem. Parasitol. 24*, 1−12.
19. Hedstrom, L., and Wang, C. C. (1990) Mycophenolic acid and thiazole adenine dinucleotide inhibition of *Tritrichomonas foetus* inosine 5′-monophosphate dehydrogenase: implications on enzyme mechanism, *Biochemistry 29*, 849−854.
20. Sintchak, M. D., Fleming, M. A., Futer, O., Raybuck, S. A., Chambers, S. P., Caron, P. R., Murcko, M. A., and Wilson, K. P. (1996) Structure and mechanism of inosine monophosphate dehydrogease in complex with the immunosuppressant mycophenolic acid, *Cell 85*, 921−930.
21. Prosise, G. L., Wu, J. Z., and Luecke, H. (2002) Crystal Structure of *Tritrichomonas foetus* Inosine Monophosphate Dehydrogenase in Complex with the Inhibitor Ribavirin Monophosphate Reveals a Catalysis-dependent Ion-binding Site, *J. Biol. Chem. 277*, 50654−50659.
22. Prosise, G. L., and Luecke, H. (2003) Crystal Structures of *Tritrichomonas foetus* Inosine Monophosphate Dehydrogenase in Complex with Substrate, Cofactor and Analogs: A Structural Basis for the Random-in Ordered-out Kinetic Mechanism, *J. Mol. Biol. 326*, 517−527.
23. Digits, J. A., and Hedstrom, L. (2000) Drug selectivity is determined by coupling across the NAD^+ site of IMP dehydrogenase, *Biochemistry 39*, 1771−1777.
24. Kerr, K. M., and Hedstrom, L. (1997) The roles of conserved carboxylate residues in IMP dehydrogenase and identification of a transition state analog, *Biochemistry 36*, 13365−13373.
25. Carter, P., and Wells, J. A. (1988) Dissecting the catalytic triad of a serine protease, *Nature 332*, 564−568.
26. Lancaster, C. R., Gross, R., and Simon, J. (2001) A third crystal form of *Wolinella succinogenes* quinol:fumarate reductase reveals domain closure at the site of fumarate reduction, *Eur. J. Biochem. 268*, 1820−1827.
27. Mowat, C. G., Moysey, R., Miles, C. S., Leys, D., Doherty, M. K., Taylor, P., Walkinshaw, M. D., Reid, G. A., and Chapman, S. K. (2001) Kinetic and crystallographic analysis of the key active site acid/base arginine in a soluble fumarate reductase, *Biochemistry 40*, 12292−12298.
28. Bossi, R. T., Negri, A., Tedeschi, G., and Mattevi, A. (2002) Structure of FAD-bound L-aspartate oxidase: insight into substrate specificity and catalysis, *Biochemistry 41*, 3018−3024.
29. Sundararaju, B., Antson, A. A., Phillips, R. S., Demidkina, T. V., Barbolina, M. V., Gollnick, P., Dodson, G. G., and Wilson, K. S. (1997) The crystal structure of *Citrobacter freundii* tyrosine phenol-lyase complexed with 3-(4′-hydroxyphenyl)propionic acid, together with site-directed mutagenesis and kinetic analysis, demonstrates that arginine 381 is required for substrate specificity, *Biochemistry 36*, 6502−6510.
30. Charnock, S. J., Brown, I. E., Turkenburg, J. P., Black, G. W., and Davies, G. J. (2002) Convergent evolution sheds light on the anti-β-elimination mechanism common to family 1 and 10 polysaccharide lyases, *Proc. Natl. Acad. Sci. U.S.A. 99*, 12067−12072.
31. Herron, S. R., Benen, J. A., Scavetta, R. D., Visser, J., and Jurnak, F. (2000) Structure and function of pectic enzymes: virulence factors of plant pathogens, *Proc. Natl. Acad. Sci. U.S.A. 97*, 8762−8769.
32. Digits, J. A., and Hedstrom, L. (1999) Species-specific inhibition of inosine 5′-monophosphate dehydrogenase by mycophenolic acid, *Biochemistry 38*, 15388−15397.
33. Clarke, A. R., Wigley, D. B., Chia, W. N., Barstow, D., Atkinson, T., and Holbrook, J. J. (1986) Site-directed mutagenesis reveals role of mobile arginine residue in lactate dehydrogenase catalysis, *Nature 324*, 699−702.
34. Kraulis, P. J. (1991) MolScript: a program to produce both detailed and schematic plots of protein structures, *J. Appl. Crystallogr. 24*, 946−950.
35. Merritt, E. A., and Bacon, D. J. (1997) Raster3D: Photorealistic Molecular Graphics, *Methods Enzymol. 277*, 505−524.

BI035823Q